



Static or dynamic pear shapes in radioactive nucleus ^{224}Rn ?

Xian-Ye Wu^{1,2} · Jin-Ze Cao¹ · Kun-Ning Zhao¹ · Zhong-Min Liu¹ · Jian Xiang³ · En-Fu Zhou⁴

Received: 6 May 2024 / Revised: 9 August 2024 / Accepted: 16 August 2024 / Published online: 14 October 2024
© The Author(s) 2024

Abstract

We report a comprehensive study on low-lying parity doublet states of ^{224}Rn by mixing both quadrupole- and octupole-shaped configurations in multireference covariant density functional theory, in which broken symmetries in configurations are restored using projection techniques. The low-lying energy spectrum is reasonably reproduced when the shape fluctuations in both the quadrupole and octupole shapes are considered. Electric octupole transition strength in ^{224}Rn is found to be $B(E3; 3_1^- \rightarrow 0_1^+) = 43$ W.u., comparable to that in ^{224}Ra , whose data are 42(3) W.u.. Our results indicate that ^{224}Rn shares similar low-energy structure with ^{224}Ra despite the excitation energy of first 3^- state of the former nucleus is higher than that of the latter. This study suggests ^{224}Rn is a candidate for the search for permanent electric dipole moment.

Keywords Covariant density functional theory · Parity doublet bands · Octupole correlations · Electric transition strengths

1 Introduction

The majority of the nuclei on the nuclear chart are characterized by reflection-symmetric shapes, either spherical or quadrupolar, in their ground states. However, atomic nuclei with a proton number Z or neutron numbers $N \simeq 34, 56, 88$, and 134 possess strong octupole correlations exhibiting

dynamical or static octupole deformations [1, 2]. Signatures of the nuclei with the static octupole-deformed shape include the presence of a low-lying positive- and negative-parity doublets as well as strong electric the dipole ($E1$) and octupole ($E3$) transition strengths. According to this criterion, the observation of a low-lying 3^- state and enhanced $E3$ transitions in the $^{144,146}\text{Ba}$ [3–5], ^{222}Ra [6], ^{224}Ra [7], and ^{226}Ra [8] suggest that these nuclei have a stable octupole deformation. By contrast, some atomic nuclei with slightly weaker $E3$ transitions but relatively larger excitation energy for the 3^- state are usually interpreted as octupole vibrators such as ^{228}Ra [6], as well as ^{208}Pb and ^{220}Rn [7]. Additionally, low-lying negative-parity states or enhanced $E1$ transitions were measured, indicating that $^{222-226}\text{Rn}$ is vibrators [9] and ^{228}Th is pear-shaped [10]. However, in suggested octupole-deformed nuclei, a strict alternation between positive and negative-parity energy levels are not observed. To draw a solid conclusion as to whether these nuclei belong to octupole rotors or vibrators, additional measurements, and comprehensive theoretical studies on these nuclei are required.

Atomic nuclei with octupole correlations have been extensively studied with various nuclear models [11–17], including self-consistent mean-field (SCMF) methods based on different energy density functionals (EDFs) [18–31] and beyond, in combination with the interacting boson models [32–35] or collective Hamiltonians [36–39]. In particular, the generator coordinate method (GCM) implemented using

This work was supported by the National Natural Science Foundation of China (Nos. 12465020, 12005802, and 12005109), the Jiangxi Provincial Natural Science Foundation (20202BAB211008), the Jiangxi Normal University (JXNU) Initial Research Foundation Grant to Doctor (12019504), the Young Talents Program under JXNU (12019870), the PhD Foundation of Chongqing Normal University (No. 23XLB010), and the Science and Technology Research Program of Chongqing Municipal Education Commission (No. KJQN202300509).

✉ Xian-Ye Wu
xywu@jxnu.edu.cn

✉ En-Fu Zhou
zhouenf@mail2.sysu.edu.cn

¹ College of Physics and Communication Electronics, Jiangxi Normal University, Nanchang 330022, China

² Jiangxi Provincial Key Laboratory of Advanced Electronic Materials and Devices, Nanchang 330022, China

³ College of Physics and Electronic Engineering, Chongqing Normal University, Chongqing 401331, China

⁴ School of Physics and Astronomy, Sun Yat-sen University, Zhuhai 519082, China

quantum-number projection techniques, including parity, particle-number, and angular momentum projections have been developed for the low-lying states of the atomic nuclei with octupole correlations based on different EDFs [40–44]. Within this multireference density functional theory (MR-DFT), it has been demonstrated that the low-lying states of ²⁰⁸Pb are multioctupole-phonon excitations [43]. By contrast, for ^{144, 146}Ba, and ²²⁴Ra, the octupole shapes of positive-parity states rapidly stabilize with an increase in spin, gradually drifting toward those of negative-parity ones [41, 42]. Given this success, we extended the MR-DFT framework to study the low-lying states of ²²⁴Rn, including the energy spectrum and electric multipole transition strengths based on relativistic energy density functional (EDF) to shed light on whether the nucleus belong to octupole rotors or vibrators.

The remainder of this paper is organized as follows. In Sect. 2, introduction to MR-DFT based on the relativistic EDF is presented. In Sect. 3, we discuss the calculation results for the low-lying states of ²²⁴Rn compared with those of ²²⁴Ra. Finally, a summary is presented in Sect. 4.

2 Theoretical framework

In MR-DFT, the nuclear wave functions of the low-lying parity doublet states are constructed as linear combinations of sets of quantum numbers projected nonorthogonal mean-field states $|\mathbf{q}\rangle$ around the equilibrium shape,

$$|\Psi_\alpha^{J^\pi}\rangle = \sum_{\mathbf{q}} f_\alpha^{J^\pi}(\mathbf{q}) \hat{P}_{MK}^J \hat{P}^N \hat{P}^Z \hat{P}^\pi |\mathbf{q}(\beta_2, \beta_3)\rangle, \tag{1}$$

where α denotes the different quantum states corresponding to a given J^π . The symbol \mathbf{q} represents the quadrupole, and octupole deformation parameters for each mean-field state. The operators \hat{P}_{MK}^J , $\hat{P}^{N,Z}$, and \hat{P}^π are used to select the components of configurations with specific quantum numbers, namely the angular momentum J , neutron (proton) number $N(Z)$, and parity $\pi = \pm$ [45].

The mean-field states $|\mathbf{q}\rangle$ are generated from the point-coupling relativistic mean-field and BCS (PC-RMF+BCS) calculations with constraints on the average nucleon numbers and quadrupole-octupole moments using the variational principle

$$\delta \langle \mathbf{q} | \hat{H} - \sum_{\tau=n,p} \lambda_\tau \hat{N}_\tau - \sum_{\lambda=1,2,3} C_\lambda (\hat{Q}_{\lambda 0} - q_\lambda)^2 | \mathbf{q} \rangle = 0 \tag{2}$$

with Lagrange multipliers λ_τ determined by the constraints $\langle \mathbf{q} | \hat{N}_\tau | \mathbf{q} \rangle = N(Z)$. The position of the center-of-mass coordinate is fixed at the origin to decouple the spurious states using the constraint $\langle \mathbf{q} | \hat{Q}_{10} | \mathbf{q} \rangle = 0$. \hat{N}_τ and $\hat{Q}_{\lambda 0} \equiv r^\lambda Y_{\lambda 0}$ are the particle-number and multipole moment operator,

respectively. q_λ is the constrained value of the multipole moment and C_λ is the corresponding stiffness constant [45]. Deformation parameters β_λ ($\lambda = 2, 3$) are defined as follows:

$$\beta_\lambda \equiv \frac{4\pi}{3AR_0^\lambda} \langle \mathbf{q} | \hat{Q}_{\lambda 0} | \mathbf{q} \rangle \tag{3}$$

with $R_0 = r_0 A^{1/3}$ and A represents the mass number of the nucleus and $r_0 = 1.2$ fm.

The weight function $f_\alpha^{J^\pi}(\mathbf{q})$ is given by Eq. (1) is determined by solving the Hill-Wheeler-Griffin: (HWG) equation [46, 47].

$$\sum_{\mathbf{q}_b} [\mathcal{H}^{J^\pi}(\mathbf{q}_a, \mathbf{q}_b) - E_\alpha^{J^\pi} \mathcal{N}^{J^\pi}(\mathbf{q}_a, \mathbf{q}_b)] f_\alpha^{J^\pi}(\mathbf{q}_b) = 0, \tag{4}$$

where the kernels are expressed as

$$\mathcal{O}^{J^\pi}(\mathbf{q}_a, \mathbf{q}_b) = \langle \mathbf{q}_a | \hat{O} \hat{P}_{KM}^J \hat{P}^\pi \hat{P}^N \hat{P}^Z | \mathbf{q}_b \rangle \tag{5}$$

with operators \hat{O} representing \hat{H} and 1 for the the Hamiltonian kernel $\mathcal{H}^{J^\pi}(\mathbf{q}_a, \mathbf{q}_b)$ and the norm kernel $\mathcal{N}^{J^\pi}(\mathbf{q}_a, \mathbf{q}_b)$.

The electric multipole transition probabilities $B(E\lambda)$ obtained from the initial state $(J_i \pi_i \alpha_i)$ into the final state $(J_f \pi_f \alpha_f)$ are calculated according to the Wigner–Eckart Theorem:

$$\begin{aligned} & B(E\lambda; J_i \pi_i \alpha_i \rightarrow J_f \pi_f \alpha_f) \\ &= \frac{e^2}{2J_i + 1} \left| \sum_{\mathbf{q}_i, \mathbf{q}_f} [f_{\alpha_i}^{J_i \pi_i}(\mathbf{q}_i)]^* [f_{\alpha_f}^{J_f \pi_f}(\mathbf{q}_f)] \right. \\ & \quad \left. \times \langle \Phi_{\alpha_f}^{J_f \pi_f}(\mathbf{q}_f) | \hat{Q}_\lambda | \Phi_{\alpha_i}^{J_i \pi_i}(\mathbf{q}_i) \rangle \right|^2 \end{aligned} \tag{6}$$

with a reduced transition matrix element,

$$\begin{aligned} & \langle \Phi_{\alpha_f}^{J_f \pi_f}(\mathbf{q}_f) | \hat{Q}_\lambda | \Phi_{\alpha_i}^{J_i \pi_i}(\mathbf{q}_i) \rangle \\ &= \delta_{\pi_i \pi_f, (-1)^\lambda} \frac{(2J_f + 1)(2J_i + 1)}{2} \sum_M \begin{pmatrix} J_f & \lambda & J_i \\ 0 & M & -M \end{pmatrix} \\ & \quad \times \int_0^\pi d\theta \sin(\theta) d_{-M0}^{J_i}(\theta) \langle \Phi(\mathbf{q}_f) | \hat{Q}_{\lambda M} e^{i\theta \hat{J}_y} \hat{P}^\pi \hat{P}^N \hat{P}^Z | \Phi(\mathbf{q}_i) \rangle, \end{aligned} \tag{7}$$

where $\hat{Q}_{\lambda M} \equiv er^2 Y_{\lambda M}$ denotes the electric multipole moment operator of rank λ . More details on the MR-DFT for quadrupole-octupole nuclei can be found in Refs. [41–44, 48, 49].

3 Results and discussions

The Dirac spinors of the nucleons are expanded in a set of harmonic oscillator basis with 14 major shells. In the PC-RMF+BCS calculations, the relativistic EDF PC-PK1 [50] was employed. Only the degrees of freedom of the axial

symmetry deformation were considered in the current study. Pairing correlations between nucleons are treated within the BCS approximation using a density-independent δ force with smooth cutoffs [51]. Strength parameters of the pairing force are set to $V_n = -349.5 \text{ MeV fm}^3$ for the neutrons and $V_p = -330.0 \text{ MeV fm}^3$ for the protons. In the calculation of the projected kernels, $N_\beta = 16$ mesh points are used for the rotation angle β , and $N_\varphi = 7$ for the gauge angle φ , both within the interval $[0, \pi]$. Since the low-lying parity doublet bands of ^{224}Rn are primarily characterized by prolate deformed configurations with $\beta_2 > 0$, the oblate deformed configurations with $\beta_2 < 0$ are excluded in the final configuration-mixing GCM calculations to reduce computational costs. The Pfaffian method [52, 53] is implemented to avoid the sign problem when calculating the norm kernel overlap.

Figure 1 presents the energies of the mean-field states for ^{224}Rn normalized to the energy minimum in β_2 - β_3 deformation plane. It is shown that, although the energy minimum is at $\beta_3 = 0$, the energy surface is soft along the β_3 direction around the minimum, which is similar to the findings in study using the relativistic Hartree–Bogoliubov (RHB) method [26]. The softness of the energy surface in ^{224}Rn is attributed to the coupling of the proton orbitals $i_{13/2} - f_{7/2}$ and the neutron orbitals $j_{13/2} - g_{7/2}$ around the the Fermi surfaces [54]. The soft behavior indicates that the dynamic correlation effects, including symmetry restoration and quadrupole-octupole shape fluctuations, can be significant in the low-lying states of ^{224}Rn .

Figure 2 shows the energy surfaces of ^{224}Rn with projections to good nucleon numbers and spin parity $J^\pi = 0^+, 1^-, 2^+, \text{ and } 3^-$. Since the mean-field configurations with very small values of β_3 are predominated by

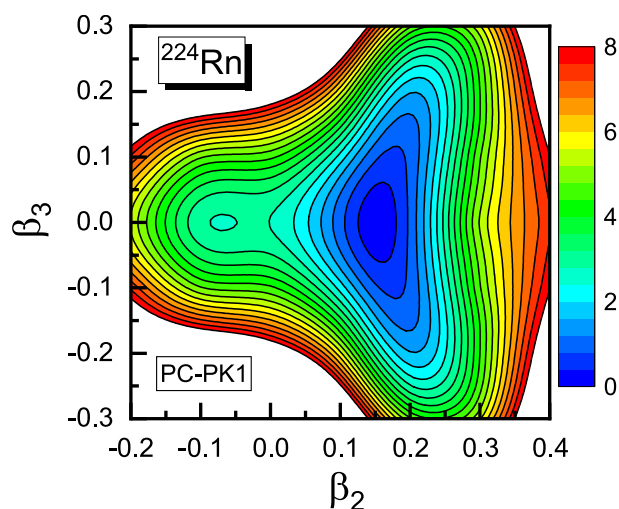


Fig. 1 (Color online) The mean-field energy surface of ^{224}Rn in β_2 - β_3 deformation plane normalized to the energy minimum. Two neighboring contour lines are separated by 0.4 MeV

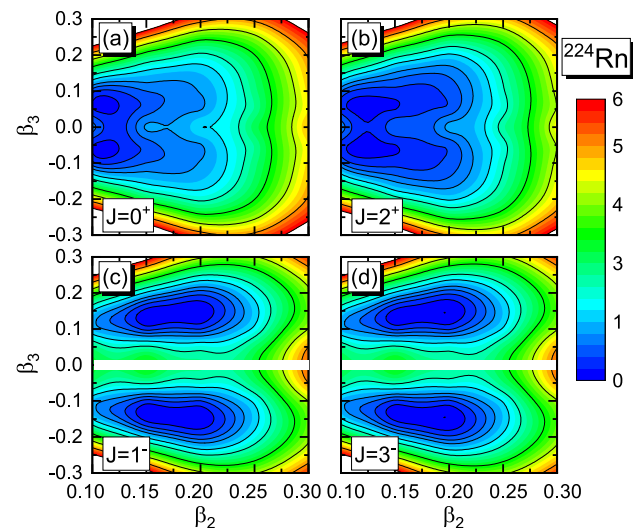


Fig. 2 (Color online) The energies of states in ^{224}Rn with projections onto good nucleon numbers, different spin parities with (a) $J^\pi = 0^+$, (b) $J^\pi = 2^+$, (c) $J^\pi = 1^-$, and (d) $J^\pi = 3^-$ in β_2 - β_3 deformation plane normalized to the energy minimum of each J state

components with positive parity, the energies of the negative-parity states projected from these mean-field configurations are not shown. The energy minimum of the 0^+ state shifts to an octupole-deformed shape with $\beta_2 = 0.1, \beta_3 = \pm 0.05$. The energy gained from the restoration of broken symmetries for the energy-minim state is $\sim 4.23 \text{ MeV}$. The energy surface of the 2^+ state is similar to that of the of 0^+ state, except that it is softer along the quadrupole deformation $\beta_2 \simeq [0.10, 0.20]$ with octupole deformation $\beta_3 \simeq [-0.10, +0.10]$. A similar result was observed in the potential energy surfaces (PESs) with $J = 1$ (cf. Fig. 2c), and $J = 3$ (cf. Fig. 2d), where the absolute minima are well separated along β_3 -direction. The projected PESs with $J = 1$ and $J = 3$ show the soft structures in octupole $\beta_3 \simeq \pm 0.15$ with a quadrupole deformation ranging from $\beta_2 \simeq 0.10$ to 0.25.

The quadrupole-octupole-deformed configurations with good quantum numbers serve as the basis for expanding the wave functions of the low-lying state within the GCM. Figure 3 shows the excitation energies of the positive- and negative-parity bands calculated by solving the HWG equations (4) for three different configuration-mixing schemes. Calculation results are compared with data from Ref. [9]. The calculation by mixing configurations with different β_2 and fixed $\beta_3 = 0.05$ provides very spread energy spectrum. In particular, the negative-parity states are very high in energy. By contrast, by mixing configurations with different β_3 values but fixed $\beta_2 = 0.15$, the energy spectrum were significantly compressed. In the full quadrupole-octupole configuration-mixing calculation, the negative-parity states shift and approached the data.

Fig. 3 (Color online) The energy spectra of low-lying states in ^{224}Rn obtained from the GCM calculations with **b** (β_2, β_3), **c** ($\beta_2 = 0.15, \beta_3$), and **d** ($\beta_2, \beta_3 = 0.05$) as generating coordinates, respectively. The data from Ref. [9] are shown in **a**

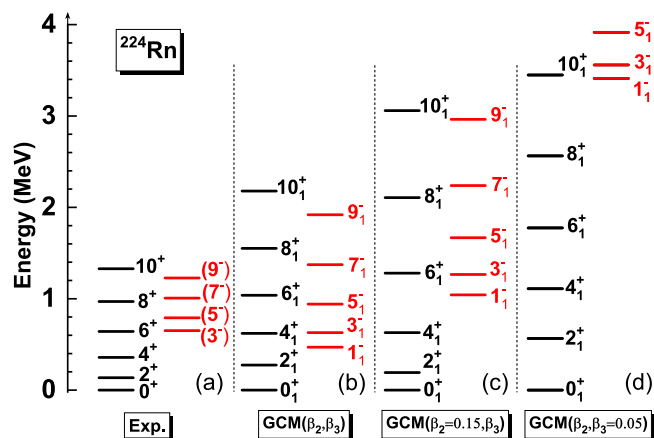


Figure 4 shows a detailed comparison of the low-lying parity doublet states including electric multipole transition strength $B(E\lambda)$. It can be observed that the results calculated using the configuration-mixing GCM (Fig. 4b) and a single energy-minimum configuration (Fig. 4c) show similar parity doublet bands with rotational characteristics. In contrast to the results of GCM calculations, the positive-parity band is more compressed in single-configuration calculations, where the negative-parity band becomes slightly lower than that obtained from GCM calculation. Quantitatively, the excitation energy $E(1^-)$ of the negative-parity band head is 0.47 MeV and 0.39 MeV from the GCM and single-configuration calculations, respectively. For the 3^- state, the calculated excitation energy $E(3^-)$ from the GCM is 0.63 MeV, which is in good agreement with the data of $E(3^-) = 0.65$ MeV. The electric octupole transition strength of ^{224}Rn is $B(E3; 3^- \rightarrow 0^+) = 43$ W.u., which is comparable to that for ^{224}Ra $B(E3; 3^- \rightarrow 0^+) = 42(3)$ W.u.. This provides evidence for the increased strength of octupole correlations in the area

surrounding $A = 224$ mass nuclei, even though the negative-parity 3^- state of ^{224}Rn has a much higher excitation energy. These results are obtained for ^{224}Ra ; however, the transition strengths are reproduced perfectly [41]. In the future experiments, it is important to further verify the calculated intraband $E2$ transitions in the same parity band, as well as the interband $E1$ and $E3$ transitions connected to the ground-state band of ^{224}Rn . This investigation indicates that the calculated energies for the excited states are slightly higher than expected. The discrepancy is likely due to the omission of triaxial and time reversal symmetry-breaking components in the model calculations, as discussed in previous studies on other nuclei with different GCM approaches [55, 56], however, when considering these symmetry breaks require consideration of the GCM calculations with cranking or particle-hole excitation configurations and the inclusion of three-dimensional angular momentum projection (3DAMP), which is beyond the framework of our proposed model.

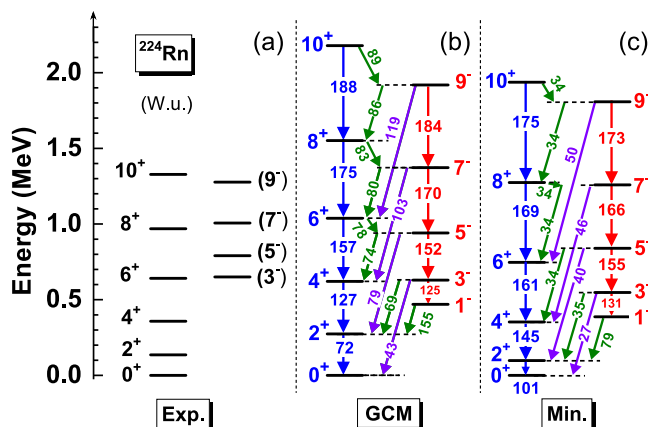


Fig. 4 (Color online) Low-lying energy spectra for ^{224}Rn . The available data are collected from Ref. [9] and the results calculated from configuration-mixing GCM and single energy-minimum configuration are shown in **a–c** columns, respectively. The numbers on the

arrows are intraband $E2$ (blue color for positive-parity and red color for negative-parity bands) and interband $E1$ (green color) or $E3$ (violet color) transition strengths connecting to the ground-state band. All transition strengths are in Weisskopf units

Fig. 5 (Color online) Collective wave functions of the parity doublet states **a** with $J^\pi = 0^+, 2^+, \dots, 8^+$ and **b** with $J^\pi = 1^-, 3^-, \dots, 9^-$ in the β_2 - β_3 deformation plane. See text for details

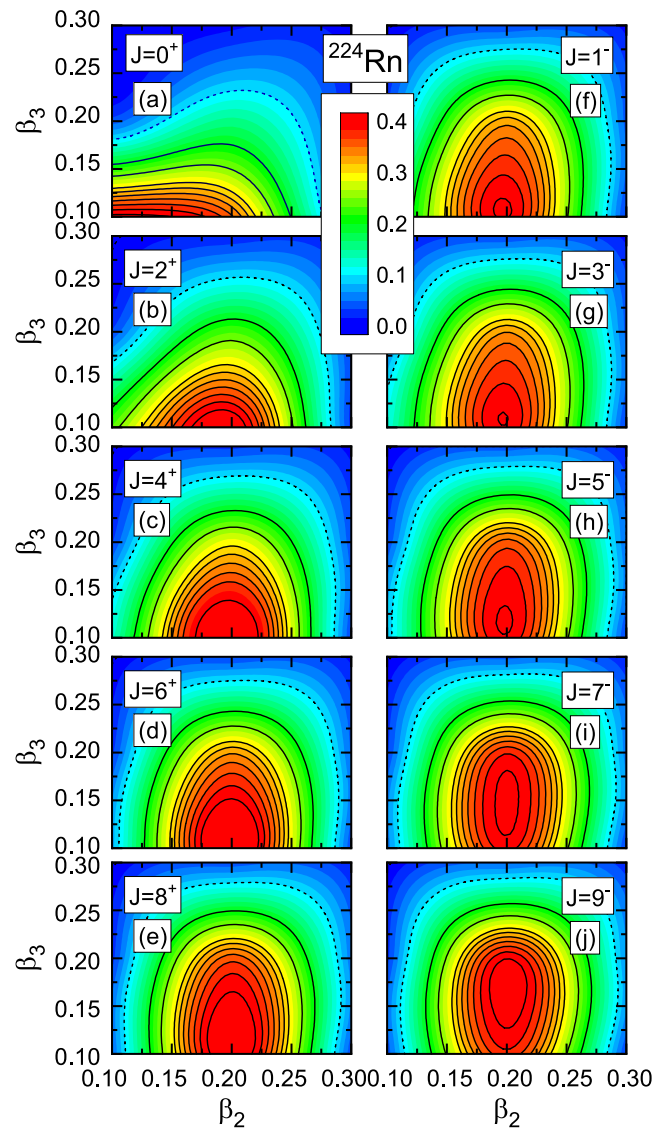


Figure 5 shows the collective nuclear wave functions $|g_\alpha^{J\pi}|^2$ for low-lying parity doublet states of the angular momentum and parity in ^{224}Rn , where the orthonormal collective wave function $g_\alpha^{J\pi}$ is constructed as

$$g_\alpha^{J\pi}(\mathbf{q}_a) = \sum_{\mathbf{q}_b} [\mathcal{N}^{J\pi}]^{1/2} f_\alpha^{J\pi}(\mathbf{q}_b). \quad (8)$$

The distribution of the collective wave functions in the β_2 - β_3 plane is usually adopted to analyze staggering behaviors in low-lying parity doublet states. The wave functions of the states become increasingly concentrated in a quadrupole-octupole-deformed configuration with an increase in angular momentum, demonstrating a picture of rotation-induced shape stabilization. Similar to ^{224}Ra [41], from the perspective of collective nuclear wave functions, the radioactive nucleus ^{224}Rn exhibits a transition from a gentle octupole deformation to a stable pear shape. We examined the

nuclear wave functions of ^{224}Rn and found that the calculations involving configurations with different β_3 and a fixed β_2 yield results similar to those of ^{224}Ra (cf. Fig. 4(e) and (f) in Ref. [41]). As the spin increases, the dominant configuration for the positive-parity states gradually shifted from weak octupole configurations to those with large octupole shapes. Conversely, for the negative-parity states, the collective wave functions are zero at $\beta_3 = 0$ and become concentrated around large octupole-deformed configurations. This corresponds with the evolution trend of the collective wave functions with the spins from the full GCM calculations, as shown in Fig. 5.

Figure 6 shows the energy ratio $R_{J/2}$ of the excitation energy of each state with an angular momentum J relative to that of positive-parity 2^+ states for ^{224}Rn . For comparison, the experimental data for ^{224}Ra are also provided. The ratio is defined as $R_{J/2} = E_x(J^\pi)/E_x(2^+)$, where $\pi = +$ and $-$ indicate positive and negative parity, respectively. The

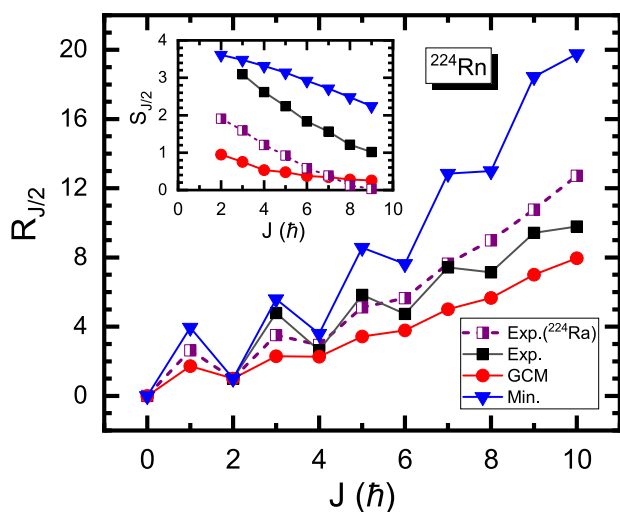


Fig. 6 (Color online) Ratio $R_{J/2}$ of the excitation energy of each J^\pm state to that of positive-parity 2^+ state as a function of the angular momentum $J(\hbar)$ for ^{224}Rn . The inset panel is the normalized staggering amplitude $S_{J/2}$ as a function of the angular momentum $J(\hbar)$. The results are calculated from configuration-mixing GCM and single energy-minimum configuration. Experimental data of ^{224}Ra [7] are also given for comparison

phenomenon of interleaving the positive- and negative-parity bands is a common method used to study the nuclei with octupole correlation. In idealized interleaving parity doublet bands, the ratio $R_{J/2}$ shows a quadratic-like function as angular momentum J increases. First, the energy levels of positive- and negative-parity bands remain decoupled, resulting in odd-even staggering and the staggering amplitude globally decreases with increasing J in ^{224}Rn . This feature is similar to that obtained from the GCM calculations for ^{224}Ra [41] and Ba isotopes [42]. The tendency of the staggering amplitude of $R_{J/2}$ as a function of the angular momentum is reproduced qualitatively for ^{224}Rn . However, the staggering amplitude deviates from the experimental data. The single energy-minimum configuration overestimates the staggering amplitude of ratio $R_{J/2}$ resulting from the lower $E(2^+)$ value of positive-parity 2^+ state obtained (cf. Fig. 4c). However, after considering the configuration-mixing effects, as shown in Fig. 4b, an overestimation of the excitation energy 2^+_1 state

Fig. 7 (Color online) **a** Theoretical and experimental excitation energies of positive-parity states in ^{224}Ra against the values in ^{224}Rn . **b** Same as **a** but for negative-parity states. The results of calculations for ^{224}Ra are taken from Ref. [41] and the available data are taken from Refs. [7, 9]

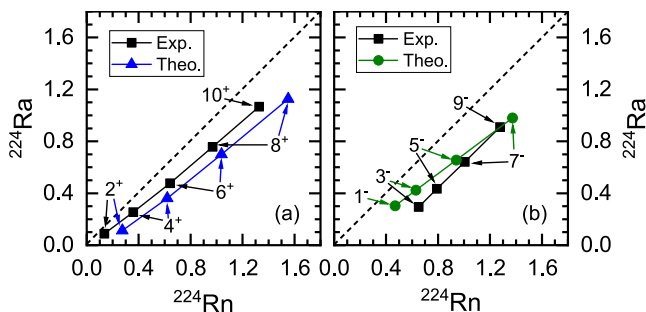
results in an underestimation of the $R_{J/2}$ -staggering amplitude in the GCM calculations. The inset panel of the Fig. 6 shows the normalized staggering $S_{J/2}$ between the positive- and negative-parity bands. It is defined as [57]

$$S_{J/2} = \left| E_x(J^\pm) - \frac{(J+1)E_x(J-1)^\mp - JE_x(J+1)^\mp}{2J+1} \right| / E_x(2^+). \quad (9)$$

Superscripts denote the parity of the two bands. This quantity reflects the octupole deformation stability changing with angular momentum $J(\hbar)$. It is clear that the normalized staggering $S_{J/2}$ decreases as the angular momentum $J(\hbar)$ increases. In brief, variations in the staggering $R_{J/2}$ and $S_{J/2}$ with increasing angular momentum $J(\hbar)$ show a behavior characteristic from octupole vibration at a lower $J(\hbar)$ to octupole rotation at a higher $J(\hbar)$ in ^{224}Rn .

Figure 7 shows the correlation between the excitation energies of ^{224}Rn and ^{224}Ra . Both the calculated and the experimental data deviated slightly from the diagonal line. As the spin increases, the excitation energies of the positive- and negative-parity states in ^{224}Rn and ^{224}Ra increased at a similar rate. In Fig. 7a, it is clear that our calculations overestimate the excitation energies of positive-parity states. However, a linear relationship of the excitation energies between ^{224}Rn and ^{224}Ra is consistent with that of experimental data. This phenomenon has also been observed in negative-parity bands, as shown in Fig. 7b. Furthermore, we plot Fig. 8 to demonstrate the relationship of the electric transition strengths between ^{224}Ra and ^{224}Rn . A linear increasing relationship is also found in the intraband transitions $B(E2; L^\pm \rightarrow (L-2)^\pm)$ or the interband transition $B(E3; L^- \rightarrow (L-3)^+)$ and $B(E1; L^- \rightarrow (L-1)^+)$ in the parity doublet bands. Moreover, for the interband $B(E1)$ and $B(E3)$ transitions between the positive- and negative-parity doublet bands, the linearity gradually deviates from the diagonal line as the spin increases, as shown in Fig. 8b. However, the intraband transitions $B(E2)$ of positive- and negative-parity bands tend to exhibit a diagonal distribution with increasing spin in Fig. 8a. It appears that the fundamental structure associated with the quadrupole-octupole correlations in ^{224}Rn exhibits similar behavior to that of ^{224}Ra .

The transition octupole moment $Q_3(3^- \rightarrow 0^+)$ can be derived from the transition matrix elements:



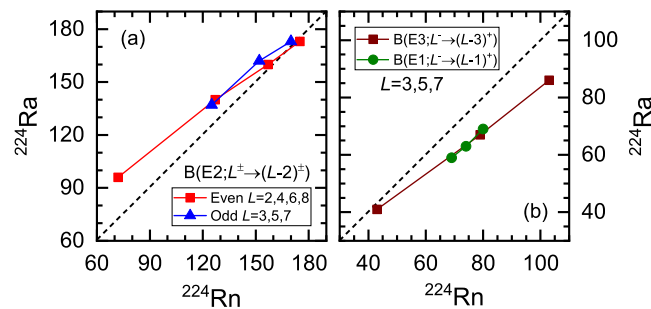


Fig. 8 (Color online) **a** Same as Fig. 7 but for electric multipole transition strengths. **a** Intraband transitions $B(E2; L^\pm \rightarrow (L-2)^\pm)$ with even $L = 2, 4, 6, 8$ and odd $L = 3, 5, 7$ stand for positive-

and negative-parity bands, respectively. **b** Interband transition $B(E3; L^- \rightarrow (L-3)^+)$ or $B(E1; L^- \rightarrow (L-1)^+)$ with $L = 3, 5, 7$ connect to parity doublet bands

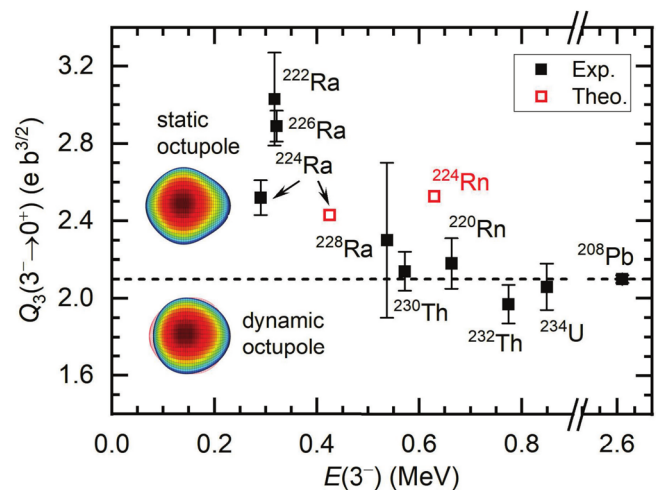
$\langle 3^- || \hat{M}(E3) || 0^+ \rangle$, which corresponds to the $3^- \rightarrow 0^+$ transitions. We plot Fig. 9 to show the relationship between the transition octupole moment $Q_3(3^- \rightarrow 0^+)$ and the energy $E(3^-)$ of the negative-parity state in ^{224}Rn , which is denoted by an open square. The solid squares show the measured Q_3 values with error bars for the nuclei with mass $A > 200$ in the $Z \simeq 88$ and $N \simeq 134$ regions, as reported in [6, 7]. For comparison, we have also included the calculated Q_3 value for ^{224}Ra , as given in Ref. [41]. ^{208}Pb has a typical dynamic pear-shaped octupole vibrator is characterized by the highest $E(3^-)$ energy with a minor Q_3 value. For the nuclei such as ^{220}Rn , $^{230, 232}\text{Th}$, and ^{234}U with similar Q_3 values to that of ^{208}Pb are considered octupole vibrators. Larger Q_3 and smaller $E(3^-)$ values for ^{222}Ra , ^{224}Ra , and ^{226}Ra indicate an enhancement in octupole collectivity that is consistent with the onset of octupole deformation in this mass region. Although a more stretched negative-parity band is obtained, our results indicate that the $E(3^-)$ energy of the experimental data is reproduced very well for ^{224}Rn [cf. Fig. 4]. The predicted transition octupole moment Q_3 of ^{224}Rn shows as larger as that of ^{224}Ra , indicating that

^{224}Rn is likely to exhibit strong octupole correlations. Therefore, ^{224}Rn has a high probability of being a rotor in our theoretical calculations. Further measurements of $Q_\lambda (\lambda = 1 \text{ or } 3)$ are required to confirm the possibility of enhanced octupole collectivity for ^{224}Rn .

4 Summary

In this study, we present a beyond-mean-field study of the low-lying parity doublet bands in ^{224}Rn with a multireference covariant density functional theory, in which the dynamic correlations related to symmetry restoration and quadrupole-octupole shape fluctuations were treated using the generator coordinate method, combined with the parity, particle-number, and angular momentum projections. The low-lying energy spectrum is reasonably reproduced when the shape fluctuations in both the quadrupole and octupole shapes are considered. Collective nuclear wave functions and the low-lying spectrum-related energy ratio $R_{J/2}$ and the normalized staggering $S_{J/2}$ suggest a transition from gentle octupole deformation to a stable pear-shaped structure. The

Fig. 9 (Color online) Relationship between the transition octupole moment $Q_3(3^- \rightarrow 0^+)$ and the energy $E(3^-)$ of the negative-parity state in ^{224}Rn , denoted by an open square. The solid squares indicate the measured Q_3 values with error bars for nuclei with mass $A > 200$ reported in [6, 7]. The calculated Q_3 value for ^{224}Ra [41] (open square) have been included for comparison. The horizontal dashed line represents the Q_3 value of octupole vibrator ^{208}Pb



results of ^{224}Rn were compared to those of ^{224}Ra . We have found these two nuclei have similar electric octupole ($E3$) transition strength. Specifically, $B(E3;3^- \rightarrow 0^+) = 43 \text{ W.u.}$ for ^{224}Rn , comparable to the experimental value of ^{224}Ra ($42(3) \text{ W.u.}$). This result indicates that ^{224}Rn may possess a similar strong octupole correlation to that in ^{224}Ra , even though the excitation energy of 3^- in ^{224}Rn is approximately twice that of ^{224}Ra . However, a more solid conclusion can only be drawn based on related octupole criteria such as the electric dipole $E1$ and octupole $E3$ transition probabilities, which will be measured in the future. This study suggests that ^{225}Rn atom, similar to ^{225}Ra atoms [58, 59], can serve as another candidate for measuring permanent atomic electric dipole moment.

Author contributions All authors contributed to the study conception and design. Material preparation, data collection, and analysis were performed by Jin-Ze Cao, Kun-Ning Zhao, and Zhong-Min Liu. The first draft of the manuscript was written by Xian-Ye Wu, and all authors commented on previous versions of the manuscript. All authors read and approved the final manuscript.

Data availability The data that support the findings of this study are openly available in Science Data Bank at <https://cstr.cn/31253.11.sciencedb.j00186.00338> and <https://doi.org/10.57760/sciencedb.j00186.00338>.

Declarations

Conflict of interest The authors declare that they have no conflict of interest.

Open Access This article is licensed under a Creative Commons Attribution 4.0 International License, which permits use, sharing, adaptation, distribution and reproduction in any medium or format, as long as you give appropriate credit to the original author(s) and the source, provide a link to the Creative Commons licence, and indicate if changes were made. The images or other third party material in this article are included in the article's Creative Commons licence, unless indicated otherwise in a credit line to the material. If material is not included in the article's Creative Commons licence and your intended use is not permitted by statutory regulation or exceeds the permitted use, you will need to obtain permission directly from the copyright holder. To view a copy of this licence, visit <http://creativecommons.org/licenses/by/4.0/>.

References

1. I. Ahmad, P.A. Butler, Octupole shapes in nuclei. *Ann. Rev. Nucl. Part. Sci.* **43**, 71 (1993). <https://doi.org/10.1146/annurev.ns.43.120193.000443>
2. P.A. Butler, W. Nazarewicz, Intrinsic reflection asymmetry in atomic nuclei. *Rev. Mod. Phys.* **68**, 349 (1996). <https://doi.org/10.1103/RevModPhys.68.349>
3. B. Bucher, S. Zhu, C.Y. Wu et al., Direct evidence of octupole deformation in neutron-rich ^{144}Ba . *Phys. Rev. Lett.* **116**, 112503 (2016). <https://doi.org/10.1103/PhysRevLett.116.112503>
4. B. Bucher, S. Zhu, C.Y. Wu et al., Direct evidence for octupole deformation in ^{146}Ba and the origin of large $E1$ moment variations in reflection-asymmetric nuclei. *Phys. Rev. Lett.* **118**, 152504 (2017). <https://doi.org/10.1103/PhysRevLett.118.152504>
5. S.J. Zhu, E.H. Wang, J.H. Hamilton et al., Coexistence of reflection asymmetric and symmetric shapes in ^{144}Ba . *Phys. Rev. Lett.* **124**, 032501 (2020). <https://doi.org/10.1103/PhysRevLett.124.032501>
6. P.A. Butler, L.P. Gaffney, P. Spagnoletti et al., Evolution of octupole deformation in radium nuclei from Coulomb excitation of radioactive ^{222}Ra and ^{228}Ra beams. *Phys. Rev. Lett.* **124**, 042503 (2020). <https://doi.org/10.1103/PhysRevLett.124.042503>
7. L.P. Gaffney, P.A. Butler, M. Scheck et al., Studies of pear-shaped nuclei using accelerated radioactive beams. *Nature* **497**, 199 (2013). <https://doi.org/10.1038/nature12073>
8. H.J. Wollersheim, H. Emling, H. Grein et al., Coulomb excitation of ^{226}Ra . *Nucl. Phys. A* **556**, 261 (1993). [https://doi.org/10.1016/0375-9474\(93\)90351-W](https://doi.org/10.1016/0375-9474(93)90351-W)
9. P.A. Butler, L.P. Gaffney, P. Spagnoletti et al., The observation of vibrating pear-shapes in radon nuclei. *Nat. Commun.* **10**, 2473 (2019). <https://doi.org/10.1038/s41467-019-10494-5>
10. M.M.R. Chishti, D. O'Donnell, G. Battaglia et al., Direct measurement of the intrinsic electric dipole moment in pear-shaped thorium-228. *Nat. Phys.* **16**, 853 (2020). <https://doi.org/10.1038/s41567-020-0899-4>
11. W. Nazarewicz, P. Olanders, I. Ragnarsson et al., Analysis of octupole instability in medium-mass and heavy nuclei. *Nucl. Phys. A* **429**, 269 (1984). [https://doi.org/10.1016/0375-9474\(84\)90208-2](https://doi.org/10.1016/0375-9474(84)90208-2)
12. P. Möller, R. Bengtsson, B.G. Carlsson et al., Axial and reflection asymmetry of the nuclear ground state. *Atom. Data Nucl. Data Tabl.* **94**, 758 (2008). <https://doi.org/10.1016/j.adt.2008.05.002>
13. T.M. Shneidman, G.G. Adamian, N.V. Antonenko et al., Cluster interpretation of parity splitting in alternating parity bands. *Phys. Lett. B* **526**, 322 (2002). [https://doi.org/10.1016/S0370-2693\(01\)01512-X](https://doi.org/10.1016/S0370-2693(01)01512-X)
14. T.M. Shneidman, G.G. Adamian, N.V. Antonenko et al., Cluster interpretation of properties of alternating parity bands in heavy nuclei. *Phys. Rev. C* **67**, 014313 (2003). <https://doi.org/10.1103/PhysRevC.67.014313>
15. N. Yoshinaga, K. Yanase, K. Higashiyama et al., Octupole phonon model based on the shell model for octupole vibrational states. *Phys. Rev. C* **98**, 044321 (2018). <https://doi.org/10.1103/PhysRevC.98.044321>
16. N. Yoshinaga, K. Yanase, C. Watanabe et al., Large-scale nuclear shell-model calculations of isotopes in the southwest region of ^{208}Pb . *Prog. Theor. Exp. Phys.* **2021**, 063D01 (2021). <https://doi.org/10.1093/ptep/ptab039>
17. X. Yin, C. Ma, Y.M. Zhao, Alternating-parity doublets of even-even Ba isotopes. *Phys. Rev. C* **109**, 024322 (2024). <https://doi.org/10.1103/PhysRevC.109.024322>
18. P. Bonche, P. Heenen, H. Flocard et al., Self-consistent calculation of the quadrupole-octupole deformation energy surface of ^{222}Ra . *Phys. Lett. B* **175**, 387 (1986). [https://doi.org/10.1016/0370-2693\(86\)90609-X](https://doi.org/10.1016/0370-2693(86)90609-X)
19. L.M. Robledo, J.L. Egido, J. Berger et al., Stable octupole deformation in some actinide nuclei. *Phys. Lett. B* **187**, 223 (1987). [https://doi.org/10.1016/0370-2693\(87\)91085-9](https://doi.org/10.1016/0370-2693(87)91085-9)
20. S. Ebata, T. Nakatsukasa, Octupole deformation in the nuclear chart based on the 3D Skyrme Hartree-Fock plus BCS model. *Phys. Scr.* **92**, 064005 (2017). <https://doi.org/10.1088/1402-4896/aa6c4c>
21. L.M. Robledo, R.R. Rodríguez-Guzmán, Octupole deformation properties of actinide isotopes within a mean field approach. *J. Phys. G* **39**, 105103 (2012). <https://doi.org/10.1088/0954-3899/39/10/105103>
22. Y. Cao, S.E. Agbemava, A.V. Afanasjev et al., Landscape of pear-shaped even-even nuclei. *Phys. Rev. C* **102**, 024311 (2020). <https://doi.org/10.1103/PhysRevC.102.024311>

23. L.-S. Geng, J. Meng, H. Toki, Reflection asymmetric relativistic mean field approach and its application to the octupole deformed nucleus ^{226}Ra . *Chin. Phys. Lett.* **24**, 1865 (2007). <https://doi.org/10.1088/0256-307X/24/7/021>
24. J.Y. Guo, P. Jiao, X.-Z. Fang, Microscopic description of nuclear shape evolution from spherical to octupole-deformed shapes in relativistic mean-field theory. *Phys. Rev. C* **82**, 047301 (2010). <https://doi.org/10.1103/PhysRevC.82.047301>
25. B.-N. Lu, J. Zhao, E.-G. Zhao et al., Multidimensionally-constrained relativistic mean-field models and potential-energy surfaces of actinide nuclei. *Phys. Rev. C* **89**, 014323 (2014). <https://doi.org/10.1103/PhysRevC.89.014323>
26. S.E. Agbemava, A.V. Afanasjev, P. Ring, Octupole deformation in the ground states of even-even nuclei: a global analysis within the covariant density functional theory. *Phys. Rev. C* **93**, 044304 (2016). <https://doi.org/10.1103/PhysRevC.93.044304>
27. S.E. Agbemava, A.V. Afanasjev, Octupole deformation in the ground states of even-even $Z \sim 96$, $N \sim 196$ actinides and super-heavy nuclei. *Phys. Rev. C* **96**, 024301 (2017). <https://doi.org/10.1103/PhysRevC.96.024301>
28. W. Zhang, Y.F. Niu, Shape transition with temperature of the pear-shaped nuclei in covariant density functional theory. *Phys. Rev. C* **96**, 054308 (2017). <https://doi.org/10.1103/PhysRevC.96.054308>
29. Y.-T. Qiu, X.-W. Wang, J.-Y. Guo, Microscopic analysis of the ground state properties of the even-even Dy isotopes in the reflection-asymmetric relativistic mean-field theory. *Phys. Rev. C* **106**, 034301 (2022). <https://doi.org/10.1103/PhysRevC.106.034301>
30. J. Yang, J. Dudek, I. Dedes et al., Exotic symmetries as stabilizing factors for superheavy nuclei: symmetry-oriented generalized concept of nuclear magic numbers. *Phys. Rev. C* **106**, 054314 (2022). <https://doi.org/10.1103/PhysRevC.106.054314>
31. Y. Su, Z.-Y. Li, L.-L. Liu et al., Sensitivity impacts owing to the variations in the type of zero-range pairing forces on the fission properties using the density functional theory. *Nucl. Sci. Tech.* **35**, 62 (2024). <https://doi.org/10.1007/s41365-024-01422-4>
32. K. Nomura, T. Nikšić, D. Vretenar, Signatures of octupole correlations in neutron-rich odd-mass barium isotopes. *Phys. Rev. C* **97**, 024317 (2018). <https://doi.org/10.1103/PhysRevC.97.024317>
33. K. Nomura, R. Rodríguez-Guzmán, L.M. Robledo et al., Evolution of octupole deformation and collectivity in neutron-rich lanthanides. *Phys. Rev. C* **104**, 044324 (2021). <https://doi.org/10.1103/PhysRevC.104.044324>
34. K. Nomura, R. Rodríguez-Guzmán, L.M. Robledo, Quadrupole-octupole coupling and the evolution of collectivity in neutron-deficient Xe, Ba, Ce, and Nd isotopes. *Phys. Rev. C* **104**, 054320 (2021). <https://doi.org/10.1103/PhysRevC.104.054320>
35. K. Nomura, Octupole correlations in collective excitations of neutron-rich $N \approx 56$ nuclei. *Phys. Rev. C* **105**, 054318 (2022). <https://doi.org/10.1103/PhysRevC.105.054318>
36. X. Zhang, Y. Peng, C.-B. Zhou et al., Nuclear alternating-parity bands and transition rates in a model of coherent quadrupole-octupole motion in neutron-rich barium isotopes. *Nucl. Sci. Tech.* **27**, 129 (2016). <https://doi.org/10.1007/s41365-016-0128-0>
37. Z.P. Li, T. Nikšić, D. Vretenar, Coexistence of nuclear shapes: self-consistent mean-field and beyond. *J. Phys. G* **43**, 024005 (2016). <https://doi.org/10.1088/0954-3899/43/2/024005>
38. Z. Xu, Z.-P. Li, Microscopic analysis of octupole shape transitions in neutron-rich actinides with relativistic energy density functional. *Chin. Phys. C* **41**, 124107 (2017). <https://doi.org/10.1088/1674-1137/41/12/124107>
39. S.Y. Xia, H. Tao, Y. Lu et al., Spectroscopy of reflection-asymmetric nuclei with relativistic energy density functionals. *Phys. Rev. C* **96**, 054303 (2017). <https://doi.org/10.1103/PhysRevC.96.054303>
40. R.N. Bernard, L.M. Robledo, T.R. Rodríguez, Octupole correlations in the ^{144}Ba nucleus described with symmetry-conserving configuration-mixing calculations. *Phys. Rev. C* **93**, 061302(R) (2016). <https://doi.org/10.1103/PhysRevC.93.061302>
41. J.M. Yao, E.F. Zhou, Z.P. Li, Beyond relativistic mean-field approach for nuclear octupole excitations. *Phys. Rev. C* **92**, 041304(R) (2015). <https://doi.org/10.1103/PhysRevC.92.041304>
42. Y. Fu, H. Wang, L.-J. Wang et al., Odd-even parity splittings and octupole correlations in neutron-rich Ba isotopes. *Phys. Rev. C* **97**, 024338 (2018). <https://doi.org/10.1103/PhysRevC.97.024338>
43. J.M. Yao, K. Hagino, Anharmonicity of multi-octupole-phonon excitations in ^{208}Pb : analysis with multireference covariant density functional theory and subbarrier fusion of $^{16}\text{O}+^{208}\text{Pb}$. *Phys. Rev. C* **94**, 011303(R) (2016). <https://doi.org/10.1103/PhysRevC.94.011303>
44. E.F. Zhou, J.M. Yao, Z.P. Li et al., Anatomy of molecular structures in ^{20}Ne . *Phys. Lett. B* **753**, 227 (2016). <https://doi.org/10.1016/j.physletb.2015.12.0280>
45. P. Ring, P. Schuck, *The Nuclear Many-Body Problem* (Springer-Verlag, Berlin, 1980)
46. D.L. Hill, J.A. Wheeler, Nuclear constitution and the interpretation of fission phenomena. *Phys. Rev.* **89**, 1102 (1953). <https://doi.org/10.1103/PhysRev.89.1102>
47. J.J. Griffin, J.A. Wheeler, Collective motions in nuclei by the method of generator coordinates. *Phys. Rev.* **108**, 311 (1957). <https://doi.org/10.1103/PhysRev.108.311>
48. J. M. Yao, "Symmetry Restoration Methods" in Handbook of Nuclear Physics, edited by I. Tanihata, H. Toki, and T. Kajino (Springer, Berlin, 2022) pp. 1–36. https://doi.org/10.1007/978-981-15-8818-1_18-1
49. E.F. Zhou, J.M. Yao, Generator coordinate method for nuclear octupole excitations: status and perspectives. *Int. J. Mod. Phys. E* **32**, 2340011 (2023). <https://doi.org/10.1142/S0218301323400116>
50. P.W. Zhao, Z.P. Li, J.M. Yao et al., New parametrization for the nuclear covariant energy density functional with a point-coupling interaction. *Phys. Rev. C* **82**, 054319 (2010). <https://doi.org/10.1103/PhysRevC.82.054319>
51. S.J. Krieger, P. Bonche, H. Flocard et al., An improved pairing interaction for mean field calculations using skyrme potentials. *Nucl. Phys. A* **517**, 275 (1990). [https://doi.org/10.1016/0375-9474\(90\)90035-K](https://doi.org/10.1016/0375-9474(90)90035-K)
52. L.M. Robledo, Sign of the overlap of Hartree–Fock–Bogoliubov wave functions. *Phys. Rev. C* **79**, 021302 (2009). <https://doi.org/10.1103/PhysRevC.79.021302>
53. G.F. Bertsch, L.M. Robledo, Symmetry restoration in Hartree–Fock–Bogoliubov based theories. *Phys. Rev. Lett.* **108**, 042505 (2012). <https://doi.org/10.1103/PhysRevLett.108.042505>
54. P.A. Butler, Octupole collectivity in nuclei. *J. Phys. G Nucl. Part. Phys.* **43**, 073002 (2016). <https://doi.org/10.1088/0954-3899/43/7/073002>
55. M. Borrajo, T.R. Rodríguez, J.L. Egido, Symmetry conserving configuration mixing method with cranked states. *Phys. Lett. B* **746**, 341 (2015). <https://doi.org/10.1016/j.physletb.2015.05.030>
56. A. Belley, J.M. Yao, B. Bally et al., Ab initio uncertainty quantification of neutrinoless double-beta decay in ^{76}Ge . *Phys. Rev. Lett.* **132**, 182502 (2024). <https://doi.org/10.1103/PhysRevLett.132.182502>
57. I. Wiedenhöver, R.V.F. Janssens, G. Hackman et al., Octupole correlations in the Pu isotopes: from vibration to static deformation? *Phys. Rev. Lett.* **83**, 2143 (1999). <https://doi.org/10.1103/PhysRevLett.83.2143>
58. R.H. Parker, M.R. Dietrich, M.R. Kalita et al., First measurement of the atomic electric dipole moment of ^{225}Ra . *Phys. Rev. Lett.* **114**, 233002 (2015). <https://doi.org/10.1103/PhysRevLett.114.233002>

59. T.E. Chupp, P. Fierlinger, M.J. Ramsey-Musolf et al., Electric dipole moments of atoms, molecules, nuclei, and particles. *Rev. Mod. Phys.* **91**, 015001 (2019). <https://doi.org/10.1103/RevModPhys.91.015001>